MONITORING THE RECOVERY PROCESS OF THE DISASTER-AFFECTED AREAS – SCALING CONTEXT IMAGE ANALYSIS IN GEO GRID-BASED SOLUTION

T. T. Vu

Grid Technology Research Center, National Institute of Advanced Industrial Science and Technology, Central 2, 1-1-1 Umezono, Tsukuba, Ibaraki, 305-8568 Japan – thuy.vu@aist.go.jp

KEY WORDS: Disaster Management, Satellite Remote Sensing, Change Detection, Image Understanding, Feature Extraction.

ABSTRACT:

This paper presents a new remotely sensed solution for monitoring the recovery of a large disaster-affected area. It exploits the powerful data grid and computing grid technologies developed on GEO (Global Earth Observation) Grid system. Accessing the ASTER portal site of GEO Grid, all the necessary ASTER multi-spectral images and on-demand ASTER digital elevation model (DEM) are easily and quickly collected. Subsequently, satellite images are automatically analyzed on a grid-based computing mechanism. The core processing is a newly developed context-based mapping approach named scaling context image analysis. Phanga province of Thailand, which was strongly attacked by the 2004 Indian Ocean tsunami, is selected as the demonstration site. Four ASTER data sets acquired on November 15, 2002 (pre-event); December 31, 2004 (just after-event); February 8, 2005 and January 26, 2006 (post-event) are used. The efficiency in data collection and data computation is the merit of the proposed solution.

1. INTRODUCTION

The increasing frequency and magnitude of natural hazards of all types are the current focus of global concern. Recent decades, the world has experienced more regularly the devastated impacts of the big earthquakes such as the 1995 Kobe, Japan earthquake, the 1999 Kocaeli, Turkey earthquake, the 2001 Gujarat, India earthquake, the 2003 Bourmedes, Algeria and the 2003 Bam, Iran earthquakes. Among the biggest earthquakes ever recorded, the M9.0 earthquake occurred off the Sumatra, Indonesia coast in December 2004 triggered a massive tsunami that caused significant damage and deaths to coastal communities in Indian Ocean. On the other hand, perhaps due to the climate change, hydro-meteorological events such as hurricane or typhoon have more frequently occurred resulting in the heavy winds, flooding, and mudslides. Numerous other events like wildfires, volcanic eruptions are also occurring worldwide. Those hazards pose a serious threat to the environment and human life.

To prepare, mitigate and respond to such large-scale disaster, the advanced remote sensing and geospatial technologies are approached (Paylor II et al. 2005). Numerous researches and several operational uses of these technologies have been carried out to see what they can really help in the disaster management cycle (Adams et al. 2004; Eguchi et al. 2000; Estrada et al. 2000; Matsuoka and Yamazaki, 1999; Singhroy and Mattar, 2000; Tralli et al. 2005; Vu et al. 2005a). It is indicated that satellite remotely sensed image is an important data source for disaster management at all stages including post-disaster responses, recovery process, preparedness, and early warning. Their wide coverage, huge archives and reasonable-temporal-resolution are significantly valuable in disaster management. They are even the only data source of the hard-hit and difficult-to-access areas at the early stage. The recent uses of satellite images have focused on the response phase, whereas a little attention has been paid in their uses for monitoring and accessing the recovery phase (Hill et al. 2006). In spite of the availability of the huge archives of satellite images nowadays, how to collect the right data sources covering the long time span is still a difficult task (Vu et al. 2007). Moreover, to be used and understood by the decision makers and the disaster management practitioners who need information not satellite images; satellite images must be accordingly analyzed.

This paper presents a solution for both retrieving and analyzing the remotely sensed data to monitor the recovery of a disaster-affected area. With the aims to be employed in large-scale disaster, the medium spatial resolution ASTER images are preferred. The time-series ASTER images are collected through GEO Grid system. The GEO (Global Earth Observation) Grid concept is the marriage of grid technology to the global earth observation. It allows the providing securely and rapidly large archives of different attribute of earth observation satellite data (ASTER, MODIS, PALSAR and etc.) and integrated service with various observation databases and geo-scientific information (www.geogrid.org). The overview of GEO Grid infrastructure is shown in Figure 1. Accessing the ASTER portal site of GEO Grid, all the necessary images of the area of interest can be easily and quickly collected. Specially, advanced digital elevation model (DEM) processing techniques implemented in GEO Grid provides ASTER DEM on user demands.

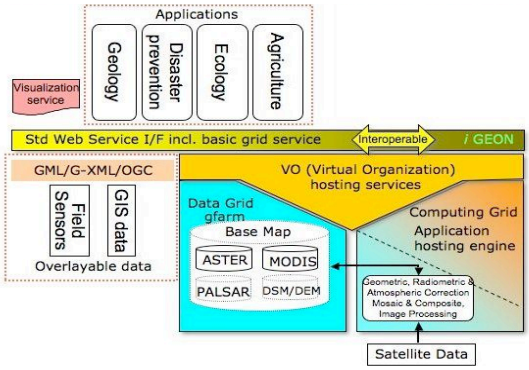

Figure 1. GEO Grid architecture - IT infrastructure (source: http://www.geogrid.org)

Data analysis exploits the powerful grid computing technology to accommodate the huge dataset required in monitoring a large affected area by a large-scale disaster. GEO Grid cluster is used as the base for implementing the scaling context time-series image analysis. It is to segment, classify and extract the objects of interest from the satellite images. Pixel-based image analysis approaches have been conventionally used to analyze the medium spatial resolution image like ASTER. Those approaches, however, solely compute the global statistics of the reflectance value in image classification and ignore the locally contextual information. As a result, it introduces the intra-region or "salt-and-pepper" error, hard to be further analyzed with other existing GIS data. The object-based and context-based approaches, hence, have been developed to overcome this drawback. The scaling context approach, which is a scale-space analysis approach, is described in Section 2. It is a further development from the author's previous works (Vu et al. 2005b; Vu et al. 2007). It is then designed for monitoring the recovery of the disaster-affected areas and being implemented on GEO Grid cluster. The details will be presented in Section 3. The long coastal area of Phanga province of Thailand, one of the extremely devastated areas by the 2004 Indian Ocean tsunami, is selected to demonstrate the proposed idea. It uses one pre-event data set (2002/11/15), one just-after event (2004/12/31), and two others after the event (2005/02/08, 2006/01/26) as illustrated in Section 4.

2. SCALING CONTEXT IMAGE ANALYSIS

Since objects appear in the ways depending on the scale of observation, the context describing them depends on the scale. Observing all the relevant information to an object on the scale-space can help to find the clue for extracting this object. The proposed method here employs the area morphology theory (Vincent, 1992) in constructing the scale-space. Briefly, area opening operation of parameter s can remove the objects smaller than s whereas area closing of parameter s can fill the holes smaller than s. Hence, applying area opening followed by area closing with a parameter s, named AOC operator, on an image is like flattening this image by parameter s. This performance segments an image into the flat zones or iso-level sets. Therefore, iterative applying AOC operator with increasing s can generate a scale-space. Figure 2 illustrates the performance of AOC operator with s = 25 and s = 81. AOC scale-space analysis is the core processing in the developed object-based extraction approach (Vu et al. 2005b; Vu et al. 2007), which solely uses the spectral bands.

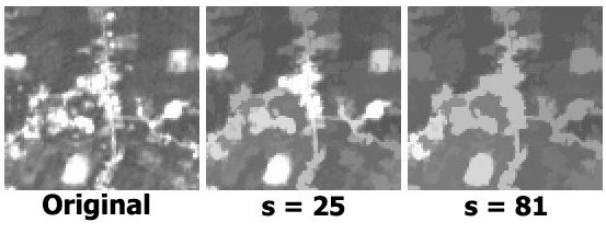

Figure 2. Illustration of AOC operator performance

Scaling context approach further extends the use of AOC scale-space. While the spectral bands are still primarily used, other relevant textural information are also integrated in the analysis as the additional channels. For instance, the edge textures of the earthquake-damaged areas show the significant discrimination to that of undamaged ones (Vu et al. 2005a) or different vegetation indexes can play an important role in presenting different attributes of the tsunami-affected areas (Kouchi and Yamazaki, 2007). Selection of those additional channels depends on the applications and the operators. The number of input channels is not limited. However, more channels require longer time computation.

Figure 3 presents the processing flowchart of the developed scaling context image analysis. Each step illustrated in this figure is implemented as an IDL script (Interactive Data Language), which is efficient in quickly implementing image-processing algorithms. After the scale-space generation as described above, K-mean clustering is employed on each scale to group the pixels into the objects with the assigned index. To assure that the same surface cover type has the same index across the scale-space, the correlation analysis is carried out. The correlation analysis, which measures the similarity between the distribution histograms of each class on the original image, is employed to find out the best match with the finest scale as the reference. Let $H_{i,0}$ is the histogram of class i on the finest scale and $H_{j,k}$ is the histogram of a class j on the scale k. Their correlation is computed as follow.

$$\rho(i,j,k) = \frac{\mathrm{cov}(H_{j,k}, H_{i,0})}{std(H_{j,k}) \times std(H_{i,0})} \quad (1)$$

where cov is the covariance of these histograms and std is the standard deviation of each histogram. The correlation values of histogram of class j on the scale k with every class on the finest scale are computed. The maximum value shows the best match and this class index on the finest scale replaces class j on the scale k.

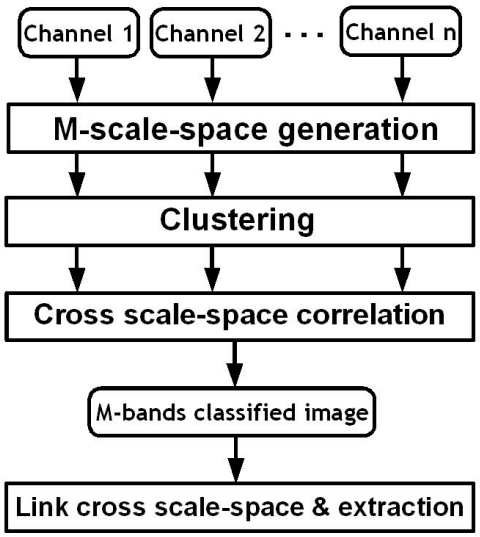

Figure 3. Flowchart of the scaling context image analysis

Across the scale-space from a coarse scale to a finer scale, an object follows the process of creation and split. Depending on the classified index, a newly created object might be a child of the current object that this new object falls into. Otherwise, this object is on its "root" scale and can be extracted. The links between objects across the scale-space are depicted in Figure 4. Let examine a three-scale-space such that *S1* is the coarsest one and *S3* is the finest one. In the current scale *S2*, there are two newly created objects named *A* and *B*. While *A* has same index to the bigger one in scale *S1*, *B* has different one. As a result, *B* can be extracted in this scale *S2* with its two-levels tree and *A* is associated with its father in *S1* and two children in *S3* to form a three-levels tree.

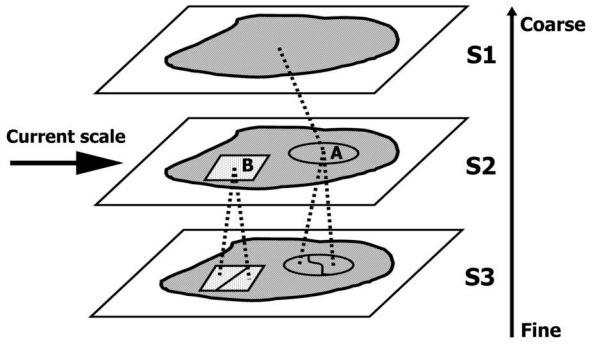

Figure 4. Illustration of the father-child relationship across the scale-space

In implementation of searching, linking and building the farther-child relationship across the scale-space, a hybrid processing on scaled images and relational database is developed. A database is prepared with the following attributes: *ID* (object id), *SCALE* (the scale it exists), *SPE* (the spectral index), *SUPID* (father's id), *SUPSCALE* (the scale father exists), *X0* and *Y0* (the starting point), *Xcen* and *Ycen* (the centre point), and *AREA* (its size). The searching is started from the finest to the coarsest scales. It collects all the adjacent pixels that have the same spectral index to form an object and assigns the *ID*. The object attributes are then recorded into the database. Subsequently, the father-child relationship is formed through assigning the father's id and father's scale into the database following the idea illustrated in Figure 4. An object that has no father will have SUPID equals 0. It is the cue for final object extraction.

The final result is a 3-bands image in which the first band presents the object ID, the second band presents the scale of the extracted objects and the third band shows their classified spectral indexes. In addition, other attributes as the results of object extraction are stored in the database. The *SUPID* and *SUPSCALE* attributes, however, can be excluded in the final database as it serves only the linking and extraction. In the case the vector format is required, the first band will be used for the conversion to ESRI shapefile format. Other attributes can be also added into the shapefile database.

Computational time is the main concern in employing the scaling context approach since the analysis integrates an enormous amount of relevant information contained in a multi-bands image. The most time consuming steps are the generation of the scale-space and the searching to link across the scale-space prior to the extraction (see Figure 3). As the processing runs on a number of scales as well as a number of bands, it seems logical that speedup could be achieved using parallel processing. For example, let assume a script runs on a N-bands image, sequentially on a single CPU, it takes $\sum_{i=1}^{N} T_i$, where T_i is the time spent on the i^{th} band. Using the simplest form of parallel processing in which each band is assigned to be carried out on a CPU, the computational time required to finish all the bands will be only $\underset{i=1}{\overset{N}{MAX}}(T_i)$, which means the maximum of all T_i values. Therefore, the computing grid system of GEO Grid is exploited for data analysis in addition to the utilization of database grid system for remotely sensed data collection. It should be noted that the GEO Grid clusters are multi-tasks operating, which means that there might be a numerous other tasks are running when a script is submitted to the cluster. The computational time would be much reduced if the clusters were running less other tasks. More details on the implementation of this scaling context image analysis specifically for the monitoring recovery application will be discussed in Section 3.

3. MONITORING THE RECOVERY OF A TSUNAMI-AFFECTED AREA

The scaling context image analysis described in Section 2 is employed as the core processing of the remotely sensed monitoring of the recovery process. The monitoring application requires the time-series multi-spectral and DEM images. The data set acquired at each time is separately analyzed by the scaling context approach. Consequently, the extracted objects form the time-series maps for comparison. The demonstration of the proposed approach used four ASTER data sets of Phanga province, Thailand, which were collected from GEO Grid portal site. These scenes were acquired on 15 November 2002, 31 December 2004, 8 February 2005 and 26 January 2006 (Figure 5). All were in the same season with the date the tsunami attacked, 26 December 2004. Approximately, their extents are 1200 pixels x 3200 pixels of 15 m spatial resolution. They are named 2002/15/11, 2004/12/31, 2005/02/08 and 2006/01/26 for the illustration in this paper.

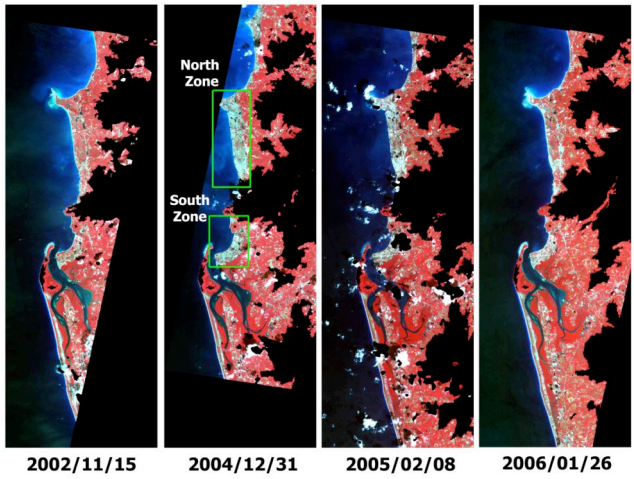

Figure 5. False colour composite images of the demonstrated area, from left to right: November 15, 2002, December 31, 2004, February 8, 2005 and January 26, 2006.

All the IDL scripts built for monitoring the tsunami-affected areas application are listed in Table 1. The processing steps were constructed in a sequential manner, which means that a script required the results of a former script as the input. Thus, the parallel processing could only take place in running each script on multi-channels of multi-data-sets. The implementation of scaling context image analysis in this paper followed the "task farming" approach. It simply means that each node runs on a data set independently and the combination will be carried out afterwards. The designed framework for implementation is depicted in Figure 6. In this figure, Ti where i= 1, 2, …, X denotes the acquisition time; Bj where j= 1, 2, …, Y denotes the band number; Sk where k= 1, 2, …, Z denotes the scale parameters. The boxes on the same row mean run in the parallel way. Details on the developed scripts and their corresponding roles in Figure 6 are described in the following paragraphs.

Script name	Parameters	Purpose
DEMMASK	DEM file name, elevation threshold	Elevation threshold
COMMONAREA	Folder name storing all the DEM files	Extract the common area from time-series data sets
IMGRESIZE	SWIR file name, new resolution (15m)	Resize an image
MASKAPPLY	File name to be masked and the result of DEMMASK	Apply a mask on an image to extract the area of interest
VICOMP	R, NIR and SWIR file names	Compute NDVI, NDSI and NDWI
MERGEBAND(1)	File names (all original bands) to be merged	Merge all bands into a multi-bands image, to form the original image
AOCSCALE	File name (single-band), object size	Compute the scaled image of parameters equals to object size
MERGEBAND(2)	File names (results of AOCSCALE) to be merged	Merge all bands into a multi-bands image, to form the image on each scale
SPECLASS	The results of MERGEBAND(2), number of classes, number of iteration	Multi-channels clustering
MANY2ONE	Folder name storing all files (results of SPECLASS), file name (result of MERGEBAND(1))	Cross scale-space correlation
SCALELINK	File name (result of MANY2ONE), text file name storing the excluded classified indexes.	Link across the scale-space and object extraction

Table 1. The implemented scripts for time-series context-based image analysis

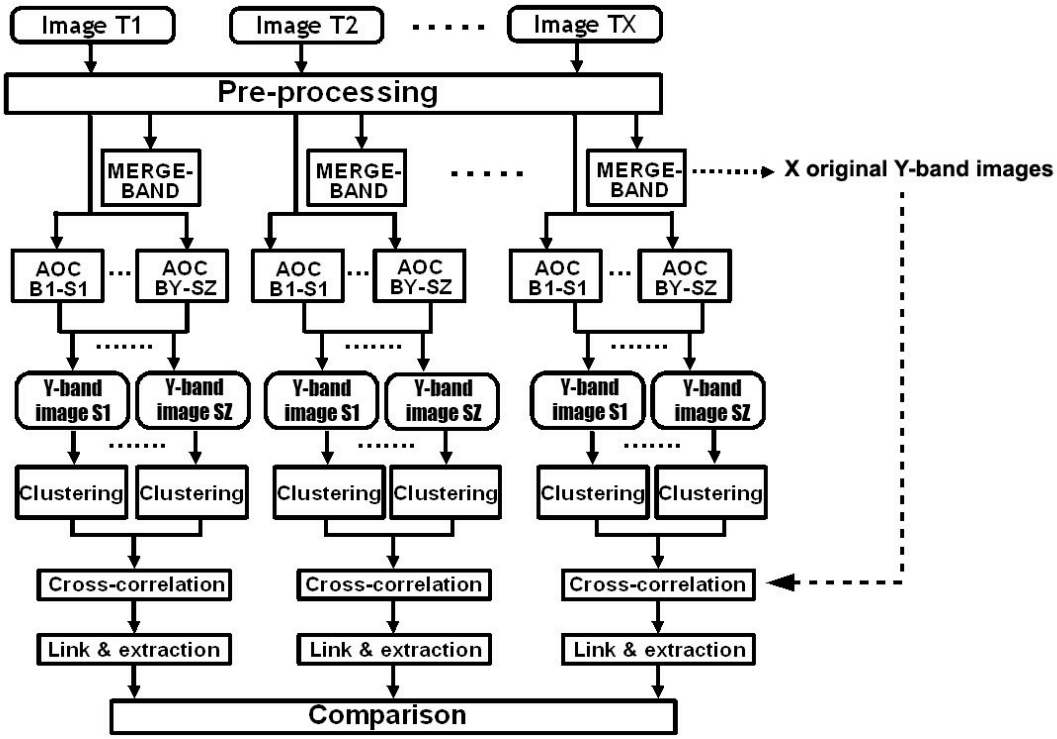

Figure 6. Time-series image analysis based on scaling context approach flowchart

To make the scaling context approach accommodate to the monitoring application, i.e. time-series image analysis, a pre-processing step (Figure 6) included five modules is required prior to the core processing. First, the elevation threshold is carried out to exclude the high elevation areas where a tsunami would not attack. Second, the common extent from the time-series DEM images is defined to crop all the analysed images. Third, the short-wave ASTER band, which is at 30 m spatial resolution, is resized to 15 m spatial resolution. As recommended by Kouchi and Yamazaki (2007), this short-wave band is used to compute the Normalized Difference Soil Index (NDSI) and Normalized Difference Water Index (NDWI) in addition to the famous Normalized Difference Vegetation Index (NDVI). Fourth, all the bands are extracted to the defined common extent from step 2. The last module of the pre-processing step is the computation of the NDVI, NDSI and NDWI. Those five modules are named DEMMASK, COMMONAREA, IMGRESIZE, MASKAPPLY, and VICOMP as shown in Table 1. It normally takes only a few seconds for each run. In the test of Phanga data, there were 4 data sets each of which contained 7 bands. Totally, 28 bands were prepared and ready for the scaling context image analysis.

The main processing started from AOCSCALE script, which could take advantage from the parallel processing. As 28 bands were prepared, 28 AOCSCALE jobs could be submitted to the

clusters. Moreover, the scale-space was generated from several scale parameters; say 4 scales, thus 28 x 4 = 112 jobs could be submitted. Likewise, 4 x 4 = 16 jobs of SPECLASS script and 4 jobs SCALELINK script respectively were submitted to run simultaneously corresponding to 4 data sets. Practically, only three most time-consuming scripts, i.e. AOCSCALE, SPECLASS and SCALELINK, were developed to utilize the parallel processing. Other scripts were submitted to compute on a single CPU and took only a few seconds for each.

Vegetation dominantly covered the test area whereas all the man-made features were very small. Therefore, only 4 scales of 9, 25, 49, and 81 for running AOCSCALE script were enough to discriminate the diverse object sizes in the scene. Regarding the parameters of the SPECLASS scripts, as a rule of thumb, a redundant number of classes and number of iterations were used, e.g. 15 classes and 15 iterations. Depending on the real data and the threshold of 5% change allowance in each class, the number of classes was determined automatically after a number of iteration. As a scene might contain the useless information such as no-data areas, the cloud and shadow, the SCALELINK required a text file listing the spectral indexes of those unused classes as the input parameter.

The extracted results by scaling context image analysis are shown in Figure 7 in which the green colours present the vegetation, and brown-red colour presents the others. In the analysis, the irrelevant classes like cloud, shadow, and water were masked out. Generally, it is easy to observe the quickest re-growth of vegetation and the slower recovery human activities. Figure 7 shows non-uniform pattern of vegetation in the 2004/12/31 and 2005/02/08 scenes unlike the other two 2002/11/15 and 2006/01/26 scenes. It inferred the effect of tsunami strike, which washed away the vegetation and resulted in more ground exposed, and the quite complete recovery of vegetation in early 2006. It was also clear that there were two distinct severe affected areas as shown in Figure 5. For the sake of illustration, they are named North and South zones.

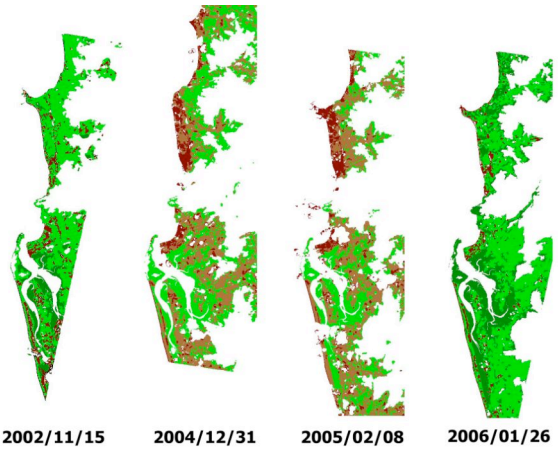

Figure 7. Extracted results of the entire areas, green colours present the vegetation cover

To more clearly illustrate the results of the scaling context analysis, a small area of the North zone was extracted as shown in Figure 8. While the upper row in this figure depicts the false-colour-composite scenes, the lower row presents the extracted objects based on their IDs. Due to the huge amount of extracted objects, the colour code is just able to show the discrimination of an object to its neighbours. Thus, the same colour of two objects that are far way each other does not mean they have the same ID. It is easy to observe the change of the biggest vegetation object. Vegetation dominated the area in the 2002/11/15 scene. Due to tsunami attack, this object was fragmented into several smaller objects as shown in the 2004/12/31 scene. It gradually reformed in the 2005/02/08 and 2006/01/26 scenes. Another observation is a water body in the top-middle of the scene. It was clearly presented as a water body in the scenes 2002, 2004, and 2005. However, it might be filled in late 2005, which was resulted in its merge with a concrete object nearby in the scene 2006/01/26.

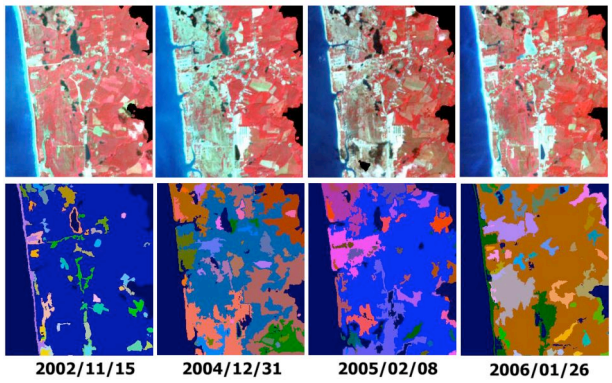

Figure 8. False colour composite (FCC) of an extracted small area in the North zone (upper row) and the extracted objects presented by their IDs (lower row).

Regarding the human activities, the small man-made objects along the coastline, which disappeared in the scenes 2004/12/31 and 2005/02/08, were recovered in the scene 2006/01/26. A bit further inland where was at the edge of affected zone, there existed a rather large concrete object in the bottom-middle of the scenes 2004/12/31, 2005/02/08 and 2006/01/26, which was not in the scene 2002/11/15. It appeared as a bright dot in FCC images in Figure 8 (the second, third and the fourth columns). Its extracted result was merged with the bare ground due to the tsunami strike in 2004/12/31 scene. Its size was reduced in 2005/02/08 scene because of the recovery activities. Finally, it was clearly discriminated from the surrounding in 2006/01/26 scene. Figure 9 depicts only the small vicinity of this concrete object to illustrate the observation. This object probably was built after 2002 and before the tsunami strike.

A small coastal area in the South zone was also extracted for investigation (Figure 10). Figure 10 shows a good match between the extracted results and the original images. In this area, less human activities in 2002/11/15 scene as vegetation dominated, which was extracted as the biggest orange object (first column of Figure 10). Due to the tsunami strike, most of vegetation was washed away and the bare ground was exposed. The vegetation object was reduced in size and the ground objects in grey and green colours dominated the scene (second column). Similar situation could be observed in the 2005/02/08 (third column). In 2006, vegetation somehow was recovered like before the disaster. However, there might be more construction in the area. The vegetation object and the concrete object are shown in grey and yellow colours, respectively in the last column of Figure 10.

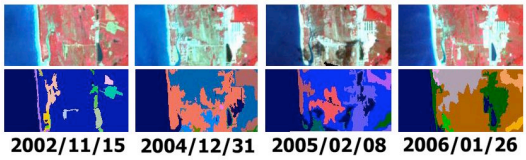

Figure 9. Observation of a concrete object in the North zone

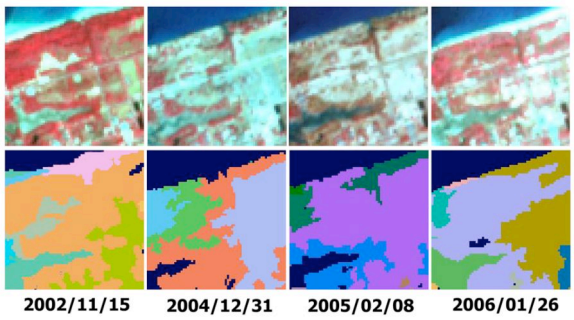

Figure 10. Observation of an area in the South zone

Grid computing is a great solution for speeding up the time-consuming processing steps. It enables the detailed and complicated context-based analysis of the large scenes in which diverse aspects of possessed information are integrated. The scaling context image analysis developed in this paper focussed in the monitoring post-disaster recovery application. However, the extracted results here show that it can generally serve as a context-based tool for image classification/segmentation and feature extraction from images of various spatial resolutions. Less number of required parameters and operator's interaction are the good points of the proposed approach.

4. CONCLUSIONS

The remotely sensed solution for monitoring the recovery after a large-scale disaster has been introduced and designed for implementation on GEO Grid infrastructures. The data collection exploited the database grid system with available free ASTER products whereas the data analysis was based on the grid-based computing power with the scaling context image analysis as the core processing. The extracted GIS-ready-to-use results would ease the works of the decision makers and disaster management practitioners. Serving the recovery process in the disaster management cycle, the automated grid-based approach on GEO Grid helps to reduce the cost invested on data and processing system. Thus, it provides a feasible solution to the developing countries, which are facing numerous large-scale disasters. The proposed approach can be easily extended to monitor the recovery after other disaster types as well as is promising for the application to the post-disaster response phase. Further works will concentrate in optimization of parallel computation on GEO Grid. Additionally, a portal site will be developed as the interface for the end-users. Scaling context image analysis generally and monitoring the disaster-affected areas particularly will be the mounted applications on GEO Grid system. The ultimate goal is to widely introduce to the users in developing countries.

ACKNOWLEDGEMENTS

The author greatly appreciates the supports of the Grid Technology Research Center in implementing the proposed approach. The research for the ASTER data described in this paper was partially supported by the Ministry of Economy, Trade and Industry in Japan.

REFERENCES

Adams, B. J., Huyck, C. K., Mansouri, B., Eguchi, R. T. and Shinozuka, M., 2004. Application of High-Resolution Optical Satellite Imagery for Post-Earthquake Damage Assessment: The 2003 Boumerdeas (Algeria) and Bam (Iran) Earthquakes. Multidisciplinary Center for Earthquake Engineering Research Progress and Accomplishments 2003-2004, University of Buffalo. http://mceer.buffalo.edu/publications/resaccom/04-SP01/12_Eguchi.pdf (accessed 20 Dec. 2007)

Eguchi, R.T., Huyck, C.K., Houshmand, B., Mansouri, B., Shinozuoka, M., Yamazaki, F. and Matsuoka, M., 2000. The Marmara earthquake: a view from space: the Marmara, Turkey earthquake of August17, 1999: Reconnaissance Report. Technical Report MCEER-00-0001 (Buffalo, NY: MCEER), pp. 151–169.

Estrada, M., Yamazaki, F. and Matsuoka, M., 2000. Use of Landsat images for the Identification of damage due to the 1999 Kocaeli, Turkey earthquake. In: *Proceeding of the 21st Asian Conference on Remote Sensing*, Singapore, pp. 1185–1190.

Hill, A. A., Keys-Mathews, L. D., Adams, B. J. and Podolsky, D., 2006. Remote Sensing and Recovery: A Case Study on the Gulf Coast of the United States. In: *Proceeding of the 4th International Workshop on Remote Sensing for Post-Disaster Response*, Cambridge, United Kingdom, CDROM.

Kouchi, K. and Yamazaki, F., 2007. Characteristics of Tsunami-Affected Areas in Moderate-Resolution Satellite Images, *IEEE Transactions on Geoscience and Remote Sensing,* 45 (6), pp.1650-1657.

Matsuoka, M. and Yamazaki, F., 1999. Characteristics of satellite images of damaged areas due to the 1995 Kobe earthquake. In: *Proceedings of the 2nd Conference on the Applications of Remote Sensing and GIS for Disaster Management*, The George Washington University, CD-ROM.

Paylor II, E. D., Evans, D. L. and Tralli, D. M., 2005. Theme issue: Remote sensing and geospatial information for natural hazards characterization. *ISPRS Journal of Photogrammetry and Remote sensing*, 59 (4), pp. 181-184.

Singhroy, V. and Mattar, K.E., 2000. SAR image techniques for mapping areas of landslides. In: *Proceedings of ISPRS Congress*, Amsterdam, The Netherlands, pp. 1395–1402.

Tralli D. M., Blom, R. G., Zlotnicki, V., Donnellan, A., Evans, D. L., 2005. Satellite remote sensing of earthquake, volcano, flood, landslide and coastal inundation hazards. *ISPRS Journal of Photogrammetry and Remote sensing*, 59 (4), pp. 185-198.

Vincent, L., 1992. Morphological area opening and closings for greyscale images. In: *Proceedings NATO Shape in Picture workshop*, Driebergen, The Netherlands, pp. 197–208.

Vu, T.T., Matsuoka, M. and Yamazaki, F., 2005a. Detection and animation of damage Using very high-resolution satellite data following the 2003 Bam, Iran, earthquake. *Earthquake Spectra*, 21(S1), pp. S319–S327.

Vu, T.T., Matsuoka, M. and Yamazaki, F., 2005b. Towards object-based damage detection. In: *Proceeding of ISPRS workshop DIMAI'2005*, Bangkok, Thailand, CDROM.

Vu, T.T., Matsuoka, M. and Yamazaki, F., 2007. Dual-scale approach for detection of tsunami-affected areas using optical satellite images. *International Journal of Remote Sensing*, 28 (13-14), pp. 2995-3011.